Atherosclerosis 290 (2019) 125–135

Contents lists available at ScienceDirect

Atherosclerosis

journal homepage: www.elsevier.com/locate/atherosclerosis

Chronological *in vivo* imaging reveals endothelial inflammation prior to neutrophils accumulation and lipid deposition in HCD-fed zebrafish

Hui Luo[a,1], Qi-qi Li[a,1], Ni Wu[b,1], Yu-ge Shen[a], Wei-ting Liao[a], Yun Yang[a], E. Dong[a], Gui-min Zhang[a], Bin-rui Liu[a], Xiao-zhu Yue[a], Xiao-qiang Tang[c], Han-shuo Yang[a,d,*]

[a] State Key Laboratory of Biotherapy and Cancer Center, West China Hospital, Sichuan University and Collaborative Innovation Center, Chengdu, China
[b] Pidu District People's Hospital, Chengdu, China
[c] Key Laboratory of Birth Defects and Related Diseases of Women and Children of MOE, State Key Laboratory of Biotherapy, West China Second University Hospital, Sichuan University, Chengdu, China
[d] Laboratory Animal Center, Sichuan University, Chengdu, China

HIGHLIGHTS

- Endothelial inflammation is prior to neutrophils accumulation and lipid deposition during the early atherogenesis.
- Endothelial inflammation is characterized by the down-regulation of *PPARγ* and the up-regulation of *TNF-α* and *IL-1β*.
- *PPARγ* agonist rosiglitazone inhibits HCD-induced up-regulation of *TNF-α* and *IL-1β* by reversing *PPARγ* expression.
- Rosiglitazone ameliorated myeloid cells/neutrophils accumulation and lipid deposition in HCD-fed zebrafish.

ARTICLE INFO

Keywords:
Hypercholesterolemia
Zebrafish
Early inflammation
Myeloid cells
Neutrophils
PPARγ

ABSTRACT

Background and aims: Hyperlipidemia-induced atherosclerosis is the major cause of heart attack and stroke in humans. However, pathological details and molecular mechanisms underlying early atherogenesis remain incompletely characterized. This study explored the early events of atherogenesis in a hypercholesterolemic zebrafish model *in vivo*.

Methods: We used transparent transgenic zebrafish larvae *Tg(lysc:EGFP)*, *Tg(mpx:EGFP)*, *Tg(mpeg1:EGFP)*, *Tg(flk1:EGFP)* or *Tg(lysc:EGFP/flk1:mCherry)*, together with fluorescently labeled control and high cholesterol diets (HCD), to dynamically investigate the early development of atherosclerosis with confocal *in vivo*. Endothelial cells with green fluorescence were sorted by fluorescence-activated cell sorting (FACS) to detect gene expression. Moreover, we treated hypercholesterolemic zebrafish model *in vivo* or human umbilical vein endothelial cells (HUVEC) *in vitro* with rosiglitazone, an agonist of peroxisome proliferator-activated receptor γ (*PPARγ*).

Results: We found that HCD-induced endothelial inflammation was an earlier pathological alteration than myeloid cells/neutrophils accumulation and lipid deposition in zebrafish vascular vessels of HCD-fed zebrafish. Endothelial inflammation was characterized by down-regulation of anti-inflammatory *PPARγ* and upregulation of pro-inflammatory tumor necrosis factor α (*TNF-α*) and interleukin-1β (*IL-1β*). Pharmacological treatment with rosiglitazone reversed the decrease in the expression of *PPARγ* and decreased expression of *TNF-α* and *IL-1β* in HCD-fed zebrafish. Moreover, rosiglitazone ameliorated myeloid cells accumulation and lipid deposition in HCD-fed zebrafish *in vivo*.

Conclusions: Hyperlipidemia-induced endothelial inflammation happens earlier than myeloid cell neutrophils accumulation in vascular vessels, and neutrophils accumulation is prior to lipid deposition during the initial stage of atherosclerosis. Early alleviation of inflammation induced by HCD would have a prophylactic effect for the initial development of atherosclerosis.

* Corresponding author. State Key Laboratory of Biotherapy and Cancer Center, West China Hospital, Sichuan University and Collaborative Innovation Center, No.17 Renmin South Road Section Three, Chengdu, Sichuan, 610041, China.
E-mail address: yhansh@scu.edu.cn (H.-s. Yang).
[1] These authors contributed equally to this article.

https://doi.org/10.1016/j.atherosclerosis.2019.09.017
Received 26 April 2019; Received in revised form 20 September 2019; Accepted 25 September 2019
Available online 27 September 2019
0021-9150/

1. Introduction

Atherosclerosis and its clinical manifestations in cardiovascular diseases are the leading cause of morbidity and mortality worldwide [1]. Atherosclerosis is attributed to the progressive narrowing of the artery lumen owing to hyperlipidemia. Recently, compelling advances in basic and clinical studies have indicated that atherosclerosis is not only a lipid storage disease, but also a complex and multifactorial process. Generally, atherosclerosis is supposed to initiate when excess cholesterol exists in blood, low-density lipoprotein cholesterol deposits in the subendothelial space, and superfluous oxidized low-density lipoprotein (ox-LDL) forms. ox-LDL results in endothelial dysfunction and monocyte recruitment into the arterial intima by pro-inflammatory factors from vascular cells [2,3]. Monocytes then differentiate into macrophages, which take up lipoproteins and become foam cells, and eventually contribute to the formation of fatty streaks—the hallmark of early atherosclerosis [4]. Fatty streaks then develop into advanced plaques that narrow the blood vessel and restrict blood flowing to the heart, brain or limbs. In addition to monocytes and macrophages, other cell types such as neutrophils have gained increasing attention recently in investigating the initiation and progression of atherosclerotic lesions [5–7]. Studies have shown that hyperlipidemia-triggered neutrophilia mediate monocyte recruitment and promotes early atherosclerosis, whereas macrophages and lesion burden decrease after neutropenia in HCD-fed *Apoe*$^{-/-}$ mice [8,9].

The treatment of atherosclerosis is considered to begin at the earliest possible stage, the fatty streak, when it is a pure inflammatory lesion [10]. Exploring the pathophysiological process and molecular mechanisms of atherosclerosis, especially the spatial and temporal details, is of utmost importance to develop potential strategies to alleviate the harm to human health [11]. However, fatty streaks develop slowly and silently, needing over decades in humans. Pathological details and molecular mechanisms underlying early atherogenesis remain controversial, mainly because of the incapability of dynamically monitoring the early occurrence of atherosclerosis in current experimental systems *in vivo*, including mouse or rabbit models and human biopsies.

Zebrafish represents a promising animal model for metabolic disease research including obesity, diabetes, fatty liver disease and atherosclerosis [12]. This animal model has greater advantages than the conventional mouse or rat models. Zebrafish larvae are small and optically transparent up to about 30 days post fertilization *in vitro*, enabling the use of fluorescently labeled lipids and fluorescent proteins to monitor cellular or subcellular events with high-resolution but without surgical or other invasive procedures in live animals. Moreover, the biochemistry and physiology of zebrafish are similar to humans in many respects. Major elements of lipid metabolism are conserved between fish and mammals [13–15]. Also, there is accelerated lipid oxidation in HCD-fed zebrafish, in which hyperlipidemia and lipid accumulation in blood vessels are rapidly induced and high levels of oxidized lipoproteins, specific oxidized phospholipid and cholesteryl ester moieties can be detected [11,16]. Many pathological events involved in early atherogenesis of zebrafish, including vascular lipid accumulation, myeloid cell recruitment, endothelial layer disorganization and other pathological processes are similar in mammals and can be reproduced and continuously monitored *in vivo* with high-resolution [11,16,17].

In the present study, we chronologically investigated the early development of atherosclerosis by taking advantage of the superiority of live optically transparent transgenic zebrafish larvae of *Tg(lysc:EGFP)*, *Tg(mpx:EGFP)*, *Tg(mpeg1:EGFP)*, *Tg(flk1:EGFP)* or *Tg(lysc:EGFP/flk1:mCherry)*. Based on clear dynamic images, we found that inflammation in endothelial cells induced by HCD happened earlier than the accumulation of myeloid cells/neutrophils in vascular vessels, and myeloid cells/neutrophils accumulation was prior to lipid deposition during the initial stage of atherosclerosis. We also revealed that down-regulation of anti-inflammatory gene expression (*PPARγ*) was critical to endothelial inflammation and up-regulation of *PPARγ* expression inhibited endothelial inflammation, blocked myeloid cells accumulation and reduced lipid retention in the vascular lumen. These results not only suggest the critical role of HCD-induced endothelial inflammation during the initiation of atherosclerosis, but also provide clues to enhance atherosclerosis therapy.

2. Materials and methods

2.1. Ethics statement

All animal work has been approved by the Sichuan Animal Care and Use Committee and conducted based on relevant guidelines. The Permit Number is SYXK (Chuan) 2008–119.

2.2. Zebrafish food preparation

HCD zebrafish food for adult or larvae was made as described before [11]. HCD food for zebrafish larvae was made by soaking baby food (Hatchfry Encapsulon Grade 0, Argent Chemical Laboratory) in a diethyl ether solution of cholesterol (Merck Millipore) to achieve a content of 4% (w/w) cholesterol in the food after ether evaporation. The control food for zebrafish larvae was only baby food without extra cholesterol addition. Adult zebrafish HCD food was made using a similar procedure but with adult fish food (Shenzhen INCH-GOLD Fish Food Co, Ltd). For purposes of studying vascular lipid accumulation in larvae, both control and HCD food were supplemented with 10 μg/g red fluorescent cholesteryl ester analog (BODIPY™ 542/563C_{11}, Invitrogen).

2.3. Zebrafish maintenance

Wild type *(AB)*, *Tg(lysc:EGFP)*, *Tg(mpx:EGFP)*, *Tg(mpeg1:EGFP)*, *Tg(flk1: EGFP)* and *Tg(lysc:EGFP/flk1:mCherry)* zebrafish were maintained in a normal condition of 28 °C, pH 7.2~7.4, 14 h on and 10 h off light cycle [18,19]. The zebrafish were randomly divided into two or more groups. HCD or control diets were fed to wild type *(AB)* or transgenic zebrafish starting at 5 weeks post fertilization (adult fish) for an additional 8 weeks or 5 days post fertilization (zebrafish larvae) for an additional 10 days twice daily.

2.4. Human umbilical vein endothelial cell isolation and culture

Endothelial cells were isolated from the veins of human umbilical cords (HUVEC) as described before [20]. Inject the 0.2% collagenase (Sigma) solution into the vein, tightly clamp it with the surgical clamp and incubate the cord in the water-bath for 10 min. Afterwards, gently squeeze the cord to facilitate cell detachment and collect the cells by washing the vein with phosphate buffer saline. Then suspend the pellet of cells in M199 medium with 20% FCS (Gibco) and culture in a 37 °C, 5% CO_2 incubator (Thermo Fischer Scientific). The following day (after less than 24 h) remove non-adherent cells by changing the culture medium. A solution with 0.25% trypsin (Gibco) was used for cell subculture.

2.5. Imaging of zebrafish larvae

For *in vivo* confocal microscopy, live larvae were anesthetized with 0.003% tricaine and embedded in a 3% methylcellulose. Lecia sp5 II confocal upright microscope system was used to take digital micrographs and pictures, which were processed with Leica LAS-AF software. Zeiss Stemi 2000-C stereomicroscope with the AxioCam MRc5 digital CCD camera was used to take whole zebrafish images.

2.6. Nile red labeling of adipose tissue

Nile red (Invitrogen) was dissolved in acetone at 1.25 mg/ml as

stock solution and stored at −20 °C avoiding smooth. Nile red was added to fish water at a final working concentration of 0.1 mg/ml, placed in the dark for 1 h and then water was changed twice before imaging.

2.7. Zebrafish and HUVEC treatment with rosiglitazone

Rosiglitazone standard was provided by Chengdu Food and Drug Administration. Rosiglitazone solution was added into the fish water at a final concentration of 0.5 μM or 1 μM from 5 days post fertilization for an additional 10 days, twice a day. HUVEC (1×10^6) were seeded in 6-well plates for 24 h before oxidized low-density lipoprotein (ox-LDL, Invitrogen) (40 μg/ml) alone or ox-LDL (40 μg/ml)/rosiglitazone (10 μM) mixture treatment for another 24 h and then cells were collected for quantitative real-time polymerase chain reaction (qPCR).

2.8. Knockout or overexpression lentivirus vector construction of PPARγ

Full length human *PPARγ* cDNA ORF was amplified from Cloning Vector (HG12019-G, Sino Biological) with BamHI or EcoRI restriction site attached to the ends, respectively. Then it was attached to the linear overexpression vector (pWPXLD) treated using the same restriction enzymes. The constructed overexpression vector is called pWPXLD-*PPARγ*. Human single guide RNAs (sgRNA) targeting *PPARγ*, #1 (5′-ctccgtggatctctccgtaa-3′) and #2 (5′-cattacgaagacattccatt-3′) were cloned into LentiCRISPRv2 plasmid [21]. The constructed knockout vector is called LentiCRISPRv2-*PPARγ*-sg1# and LentiCRISPRv2-*PPARγ*-sg2#.

2.9. HUVEC knockout or overexpression of PPARγ by lentivirus infection

Lentivirus was prepared by co-transfection of 293T cells with overexpression or knockout of the above plasmid along with packaging plasmids pMD2.G (AddGene) and psPAX2 (AddGene) [22]. Lentivirus-containing medium was collected at 48 and 72 h post-transfect- ion, filtered using a 0.45 μm filter and stored at −80 °C. For viral transduction, HUVEC were incubated with lentivirus-containing medium and 10 μg/mL polybrene for 24 h. HUVEC were allowed to recover for 24 h before treatment with ox-LDL (40 μg/ml) for another 24 h. Overexpression or knockout of *PPARγ* in HUVEC was validated by reverse transcription polymerase chain reaction (RT-PCR) or DNA sequencing.

2.10. Fluorescence-activated cell sorting (FACS) of transgenic zebrafish endothelial cells

The HCD or control diet was fed to *Tg(flk1: EGFP)* larvae starting at 5 days post fertilization for an additional 6 days, twice daily. For each sample, ~50–100 larvae were stored and dissociated by collagenase I (Sigma) (1 mg/ml) for 25~30 min at 31 °C. Single-cell suspensions were filtered using a 40 μm mesh and stained with 4′,6-diamidino-2-phenylindole (DAPI, Invitrogen) (1 μg/ml) for 10~20 min at 37 °C. At least 10,000 endothelial cells with green fluorescence were sorted using an Aria III flow cytometer (BD Biosciences) [23].

2.11. Quantitative real-time PCR for gene expression

Total RNA of larvae and HUVEC were isolated using TRIZOL Reagent (Invitrogen) according to the instructions. Quantity and quality (A260/A280 ratio) of isolated RNA were determined with a NanoDrop ND2000 spectrophotometer (Thermo Fischer Scientific). Endothelial cells sorted from larvae were isolated by single cell real time reverse transcription polymerase chain reaction (RT-PCR) assay kit (Signosis). All cDNA synthesis was performed by Revert Aid RT Kit (Thermo Fischer Scientific) according to the instructions. qPCR was performed on a CFX96™ Real-Time PCR Detection System (Bio-Rad) with SYBR green fluorescent labeled qPCR mix (Bio-Rad) and run with cycling parameters: 95 °C (30s), 40 cycles of 95 °C (5s), 60 °C (30s) and then 65°C–95 °C, increasing 0.5 °C per 5s. All qPCR primers used (Supplementary Table 1). The real-time PCR results were analyzed by Bio-Rad CFX Manager 2.0 software.

2.12. Microarray expression profile of zebrafish

The RNA samples extracted using Trizol reagent (Invitrogen) were sent to CapitalBio Beijing, China, for microarray hybridization on Affymetrix Zebrafish Genome Array containing 15,617 transcripts (Affymetrix). All manipulations were performed as described in the technical manual (Affymetrix). Hybridization data were analyzed using GeneChip Operating Software (GCOS 1.4). The images were first assessed by visual inspection and then analyzed to generate raw data files saved as CEL files using the default setting of GCOS 1.4. Then, CEL files were analyzed for data summarization, normalization and quality control using the GeneSpring sofware with MAS5 algorithm. Gene sets regarding zebrafish lipid metabolism pathway were collected in Kyoto Encyclopedia of Genes and Genomes (KEGG). These identified genes mapping to the microarray expression profile of zebrafish feeding with HCD or control diets for 10 days were visualized by heat maps.

2.13. Statistical analysis

Statistical analysis was done with Imaris 9.1.0 and SPSS 18.0 statistical analysis software with unpaired student's *t*-test, $\alpha = 0.05$, 0.01 or 0.001. It is regarded as statistically significant at $p < 0.05$. Graph Pad Prism 5 was used for figures.

3. Results

3.1. Myeloid cells accumulated near to vascular vessels in zebrafish larvae fed HCD

HCD-induced hypercholesterolemia in mice resulted in apparent thickening of the endothelial cell layer in early lesions [24]. We also observed thicken endothelial cell layers, especially at sites of intestinal blood vessel bifurcations (Fig. 1A), and red fluorescent plaques in dorsal aorta (Fig. 1C) in *Tg(flk1:EGFP)* transgenic larvae fed red fluorescence-labeled HCD for 10 days. The analysis of gene expression profiles showed that fifteen pathways relating to lipid metabolism changed in HCD-fed zebrafish. Among them, pathways of fatty acid elongation (Supplementary Fig. 2A), fatty acid degradation (Supplementary Fig. 2B), arachidonic acid metabolism (Supplementary Fig. 2C) and biosynthesis of unsaturated fatty acids (Supplementary Fig. 2D) up-regulated significantly. Moreover, we found that zebrafish had an enlarged belly (Supplementary Fig. 1A) and body weight increased significantly ($p < 0.05$) (Supplementary Fig. 1B) after feeding HCD food for an additional 8 weeks starting at 5 weeks post fertilization ("adult" fish). These results indicated that zebrafish are inherently susceptible to HCD diets.

Myeloid cells, macrophages or neutrophils, play important roles during atherogenesis [6,25]. To observe the recruitment of myeloid cells in early atherogenesis in HCD-fed zebrafish larvae, we used *Tg(lysc:EGFP)* transgenic larvae in which EGFP expression is driven by lysozyme C promoter and mainly expressed in macrophages or neutrophils [26]. After 10 days of HCD feeding from 5 days post fertilization, green fluorescent myeloid cells accumulated in the trunk where seemed to be the position of the caudal vein, which was different from diffuse distribution in control fish (Supplementary Fig. 1C). To further reveal the spatial relationship between the caudal vein and recruited myeloid cells, we used *Tg(lysc:EGFP/flk1:mCherry)* double transgenic zebrafish larvae. In this model, myeloid cells (green) and endothelial cells (red) could be simultaneously investigated under fluorescent microscope at high-resolution. After 10 days of HCD feeding, the imaging clearly showed that green myeloid cells accumulated along the caudal

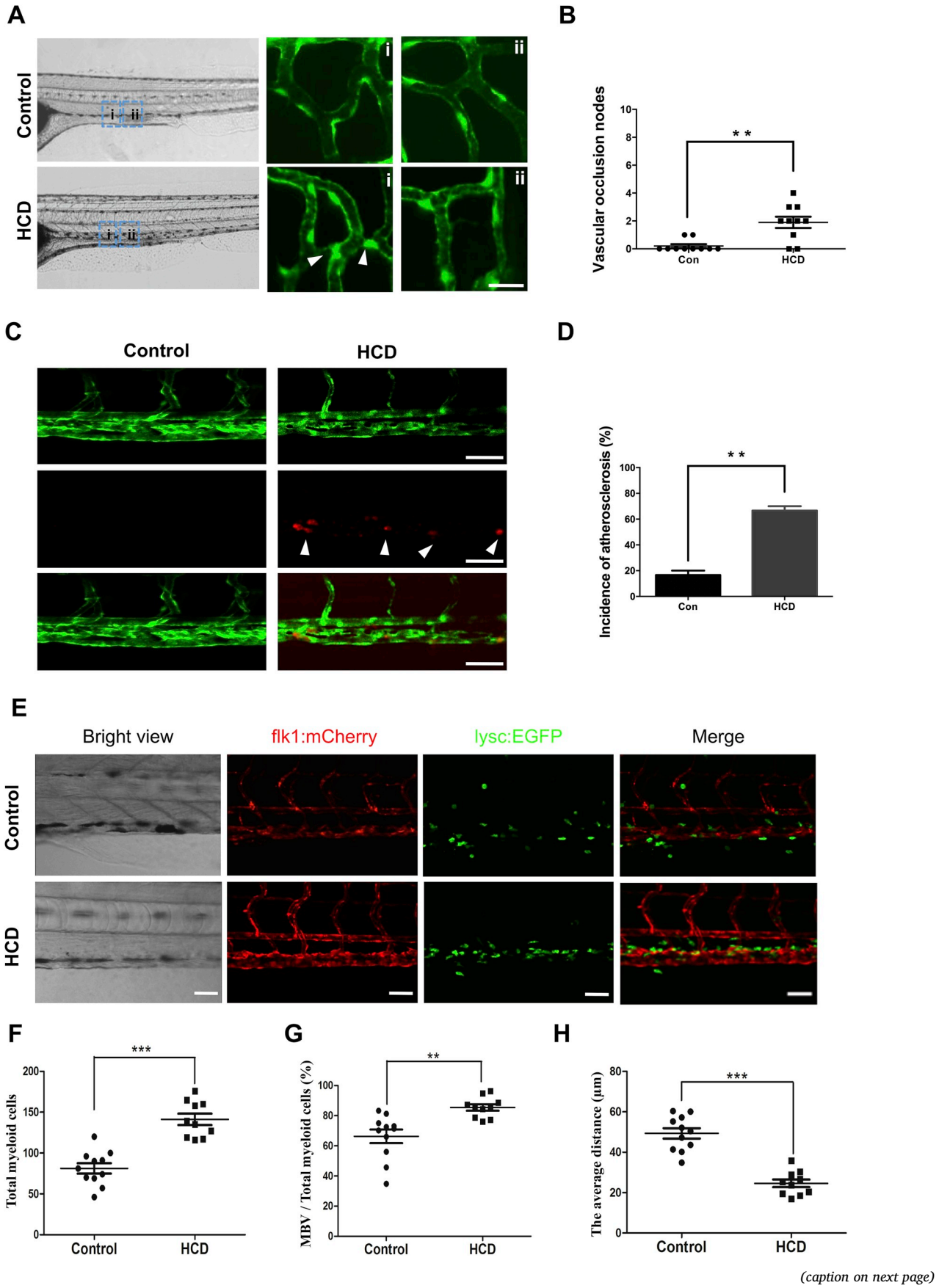

(caption on next page)

Fig. 1. Myeloid cells accumulate near vascular vessels in high cholesterol diet (HCD) fed zebrafish.
(A) Confocal images of vessel (green) bifurcation (i ii) in *Tg(flk1:EGFP)* larvae. White arrowheads, incrassate endothelial cells layer. Scale bar, 20 μm. (B) Vascular occlusion nodes, statistical analysis of incrassate endothelial cells layer of vessel (green) bifurcation (i ii). (C) Confocal images of the dorsal aorta (green) in *Tg (flk1:EGFP)* larvae. White arrowheads, enhanced red fluorescent lipid plaques. Scale bar, 50 μm. (D) Incidence of atherosclerosis, percentage of zebrafish with atherosclerosis *versus* total zebrafish in the control or HCD group. (E) Confocal images of caudal vein in *Tg(lysc:EGFP/flk1:mCherry)* larvae, and myeloid cells (green) accumulation along the vessel (red) walls. Scale bar, 50 μm. (F) Statistical analysis of total myeloid cells in the region from yolk sac to tail. (G) Percentage of myeloid cells between the caudal vein and dorsal aorta (MBV) *versus* total myeloid cells. (H) Average distance of myeloid cells to caudal vein. All images and statistical analysis were carried out after feeding zebrafish with red fluorescently labeled control or HCD diets for 10 days, starting at 5 days post fertilization. $^{**}p < 0.01$; $^{***}p < 0.001$, Student's t-test.

vein and dorsal aorta (Fig. 1E). Quantitative analysis showed that significantly increased in myeloid cells number ($p < 0.001$) (Fig. 1F) and a higher percentage of myeloid cells accumulated between the caudal vein and dorsal aorta (MBV) ($p < 0.01$) (Fig. 1G) and closer to the caudal vein ($p < 0.001$) (Fig. 1H).

3.2. Myeloid cells recruitment preceded vascular lipid deposition

In addition to myeloid cells recruitment, lipid retention in vascular walls is another important event during early atherogenesis [27,28]. To reveal the chronological order of myeloid cells recruitment and lipid retention during the initial stage of atherosclerosis, we fed *Tg(lysc:EGFP)* transgenic larvae with control or HCD food supplemented with 10 μg/g red fluorescent cholesteryl and monitored myeloid cells recruitment (green) and lipid retention (red) every day by confocal microscope. Dynamic observations clearly showed that as early as 8 days myeloid cells began to recruit to vascular vessels (Fig. 2A) and a higher percentage of myeloid cells accumulated between the caudal vein and dorsal aorta (MBV) ($p < 0.05$) (Fig. 2C) and closer to the caudal vein in HCD-fed larvae ($p < 0.01$) (Fig. 2D). Vascular lipid retention (Fig. 2A) and increase in total myeloid cells could not be detected until 10 days ($p < 0.05$) (Fig. 2B). These results indicated that myeloid cells recruitment to vasculature is prior to vascular lipid retention in HCD-fed zebrafish larvae.

3.3. Neutrophils not macrophages accumulated before vascular lipid deposition

Lysc-EGFP cells include macrophages and neutrophils [26]. To discriminate whether macrophage or/and neutrophil responded to HCD feeding, we used two more specific transgenic zebrafish *Tg(mpx:EGFP)* and *Tg(mpeg1:EGFP)*. In *Tg(mpx:EGFP)*, the neutrophil-specific protein myeloperoxidase (mpx) promoter drives EGFP expression in neutrophils [29]. Macrophage expressed gene 1 (mpeg1) was identified as tightly restricted to macrophages and has been used as a marker for this cell lineage in zebrafish [30,31]. Using these two genetically modified zebrafish, a similar phenomenon to *Tg(lysc:EGFP)* (Fig. 2A) was observed in *Tg(mpx:EGFP)* (Fig. 3A) but not in *Tg(mpeg1:EGFP)* (Supplementary Fig. 3A). In *Tg(mpx:EGFP)* zebrafish, we found that neutrophils between the caudal vein and dorsal aorta (NBV) increased significantly ($p < 0.05$) (Fig. 3C) and closer to the caudal vein ($p < 0.05$) (Fig. 3D) from day 8. In transgenic zebrafish *Tg(mpeg1:EGFP)*, the total number of macrophages ($p > 0.05$) (Supplementary Fig. 3B), the percentage of macrophages between the caudal vein and dorsal aorta ($p > 0.05$) (Supplementary Fig. 3C) and the average distance from the macrophage to the caudal vein ($p > 0.05$) (Supplementary Fig. 3D) did not significantly change. Thus, neutrophils rather than macrophages may be the cells that accumulate near vasculatures before vascular lipid deposition.

3.4. PPARγ down-regulation in HCD-fed zebrafish larvae and endothelial cells prior to myeloid cells accumulation

Myeloid cells accumulation suggested that HCD induced an inflammatory response in zebrafish large vascular vessels. Given that TNF-α and IL-1β are two major cytokines that trigger the down-stream inflammatory cascade during hypercholesterolemia-induced innate immune response [32], we detected *TNF-α* and *IL-1β* expression in zebrafish larvae by quantitative RT-PCR (RT-qPCR) after feeding HCD or control diets for 10 days. Results showed that both *TNF-α* ($p < 0.01$) and *IL-1β* (p$p < 0.05$) expression significantly increased (Fig. 4A).

PPARγ plays an important role in endothelial cell homeostasis [33] and acts as an anti-inflammatory regulator in human diseases [34,35]. So, we detected *PPARγ* expression and found that it significantly decreased in HCD-fed larvae ($p < 0.05$) (Fig. 4B). We further collected endothelial cells at different time (0,3,5,7,9 days) by fluorescence-activated cell sorting post HCD or control diets feeding (Fig. 4C). RT-qPCR detected the chronological expression of *PPARγ* in sorted endothelial cells and indicated that *PPARγ* was slightly but not significantly decreased at 5 days ($p > 0.05$) but significantly decreased at 7 and 9 days in HCD-fed larvae ($p < 0.05$) (Fig. 4D). Therefore, we further detected the expression of *PPARγ* at 6 days and found it significantly decreased ($p < 0.05$) (Fig. 4E). Meanwhile, the expression of *TNF-α* was significantly increased ($p < 0.05$) (Fig. 4F) at 6 days. Thus, this indicates that the decrease of *PPARγ* expression in endothelial cells was earlier than myeloid cells accumulation (Fig. 4G). Moreover, in human umbilical cords cells (HUVEC) treated with ox-LDL for 24 h, *PPARγ* expression decreased ($p < 0.05$) (Fig. 4H) while *TNF-α* (p$p < 0.01$) (Fig. 4I) and *IL-1β* ($p < 0.05$) (Fig. 4J) expression increased. This is consistent with observations in zebrafish.

Adipose cells could secret a variety of pro-inflammatory and inflammatory cytokines [36] and HCD made adult zebrafish fatter (Supplementary Fig. 1A). To reveal whether myeloid cells were recruited by adipose cells, we detected adipocytes in zebrafish larvae after 10 days of control or HCD diets by Nile red staining. Red fluorescent imaging indicated that no obvious differences were observed between the control and HCD-fed larvae and also no red fluorescent signaling was detected in the region where myeloid cells accumulated (Supplementary Fig. 4A). Anti-inflammatory gene CCAAT/enhancer-binding protein β (*C/EBP-β*) ($p < 0.05$) (Supplementary Fig. 4B) and *PPARγ* (p$p < 0.05$) (Fig. 4B) expression significantly decreased. p RT-qPCR results revealed that zebrafish adipocyte lineage markers *leptin-α* and fatty acid-binding protein-11α (*Fabp-11α*) had no significant up-regulation in HCD-fed zebrafish ($p > 0.05$) (Supplementary Fig. 4C). Together, these results suggested that HCD-induced up-regulation of *TNF-α* ($p < 0.01$) and *IL-1β* ($p < 0.05$) (Fig. 4A) expression in zebrafish larvae was not related to the increase of adipose cells.

3.5. PPARγ agonist rosiglitazone ameliorated inflammation, myeloid cells accumulation and lipid deposition in zebrafish larvae in vivo

Then, we investigated whether up-regulation of *PPARγ* could ameliorate inflammation and inhibit myeloid cells accumulation and lipid deposition. By studying the anti-inflammatory effect of rosiglitazone in HCD-fed zebrafish, we found that rosiglitazone significantly ameliorated myeloid cells accumulation near the caudal vein and dorsal aorta (Fig. 5A). Rosiglitazone (1 μM) significantly increased *PPARγ* expression ($p < 0.05$) (Fig. 5B) and reduced *TNF-α* and *IL-1β* expression ($p < 0.05$) (Fig. 5C) in zebrafish fed HCD. Quantitative analysis of the distance of myeloid cells to the caudal vein ($p < 0.01$) (Fig. 5E) and the percentage of myeloid cells between the dorsal aorta and caudal vein to total myeloid cells ($p < 0.01$) (Fig. 5F) indicated precovery of

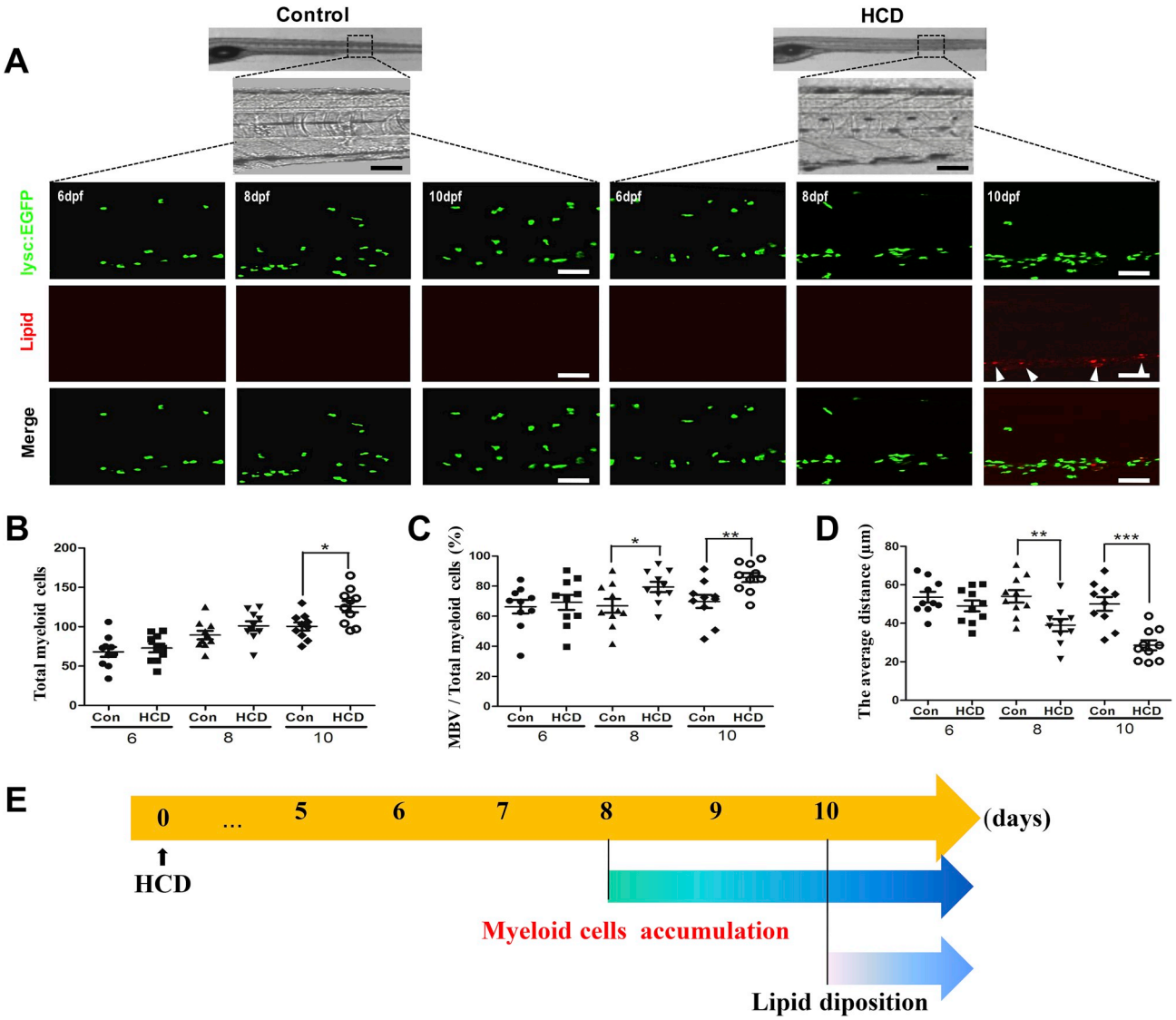

Fig. 2. Myeloid cells recruitment precedes vascular lipid deposition.
(A) Confocal images of caudal vein in *Tg(lysc:EGFP)* larvae. Myeloid cells (green) and lipid deposition plaques (red) distributed as indicated. White arrowheads, enhanced red fluorescent lipid plaques. Scale bar, 50 μm. Days post feeding (dpf). (B) Statistical analysis of total myeloid cells in the region from yolk sac to tail. (C) Percentage of myeloid cells between the caudal vein and dorsal aorta (MBV) *versus* total myeloid cells. (D) Average distance of myeloid cells to caudal vein. (E) Schematic diagram of the chronological order of myeloid cells accumulation and lipid deposition. All images and statistical analysis were carried out after feeding zebrafish with red fluorescently labeled control or HCD diets for 6, 8 and 10 days, starting at 5 days post fertilization. $*p < 0.05$; $**p < 0.01$; $***p < 0.001$, Student's t-test. (For interpretation of the references to colour in this figure legend, the reader is referred to the Web version of this article.)

myeloid cells distribution in dispersion degree. Rosiglitazone treatment did not suppress HCD-induced increase of myeloid cells total number ($p > 0.05$) (Fig. 5D), suggesting the *PPARγ*-independent mechanism caused the increase of myeloid cells number. Moreover, rosiglitazone (1 μM) treatment almost completely blocked the lipid deposition in *Tg (flk1:EGFP)* larvae fed red fluorescently labeled control or HCD diets (Fig. 5G). Together, these results indicated that extinguishing *PPARγ*-mediated inflammation could ameliorate HCD-induced myeloid cells accumulation and lipid deposition in zebrafish, suggesting the prophylactic potential of targeting *PPARγ* to inhibit early development of arteriosclerosis.

Next, we examined the anti-inflammatory effect of rosiglitazone to ox-LDL induced inflammation in HUVEC. In ox-LDL treated HUVEC cells, *TNF-α* ($p < 0.01$) (Fig. 5H) and *IL-1β* ($p < 0.05$) (Fig. 5I) expression increased and *PPARγ* expression ($p < 0.05$) (Fig. 5J) decreased significantly. However, after the addition of rosiglitazone, *TNF-α* ($p < 0.05$) (Fig. 5H) and *IL-1β* ($p < 0.05$) (Fig. 5I) expression decreased and *PPARγ* expression ($p < 0.05$) (Fig. 5J) increased significantly compared to ox-LDL treated HUVEC cells. In addition, we tested the effect of *PPARγ* overexpression or knockout on the expression of *TNF-α* and *IL-1β*. We overexpressed ($p < 0.01$) (Supplementary Fig. 5A) or knocked out (Supplementary Fig. 6A) *PPARγ* gene by using recombinant lentivirus infection in HUVEC cells. The results showed that *PPARγ* overexpression significantly inhibited upregulation of *TNF-α* ($p < 0.01$) (Supplementary Fig. 5B) and *IL-1β* ($p < 0.01$) (Supplementary Fig. 5C) expression in HUVEC cells after ox-LDL treatment. In *PPARγ* knockout HUVEC cells, ox-LDL treatment further promoted the expression of *TNF-α* ($p < 0.01$) (Supplementary Fig. 6B) and *IL-1β* ($p < 0.05$) (Supplementary Fig. 6C). Together, these pieces of evidence suggested that *PPARγ* could directly inhibit the expression of inflammatory genes.

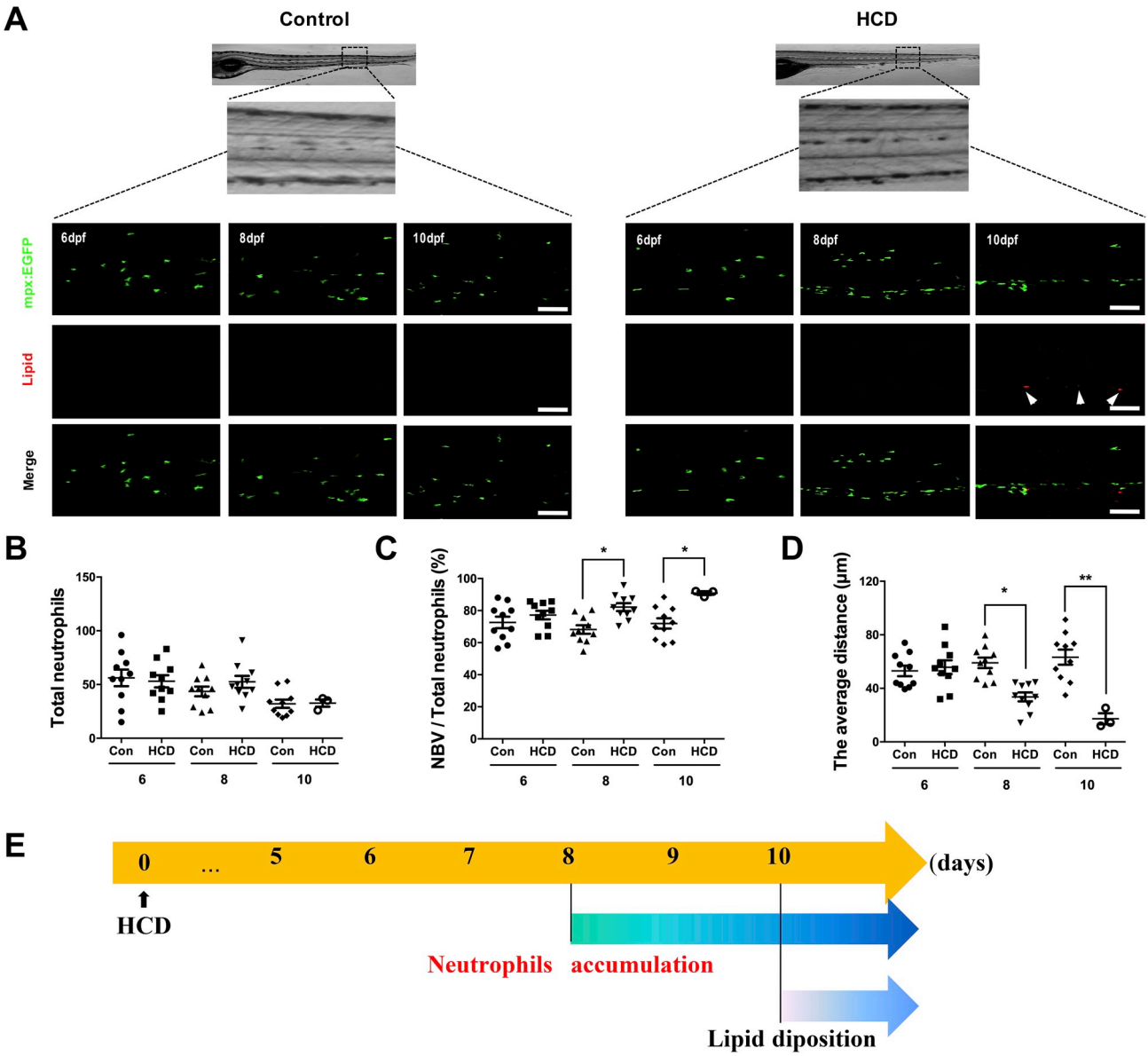

Fig. 3. Neutrophils accumulate before vascular lipid deposition.
(A) Confocal images of the caudal vein in *Tg(mpx:EGFP)* larvae. Neutrophils (green) and lipid deposition plaques (red) distributed as indicated. White arrowheads, enhanced red fluorescent lipid plaques. Scale bar, 25 μm. Days post feeding (dpf). (B) Statistical analysis of total neutrophils in the region from yolk sac to tail. (C) Percentage of neutrophils between the caudal vein and dorsal aorta (NBV) *versus* total neutrophils. (D) Average distance of neutrophils to caudal vein. (E) Schematic diagram of the chronological order of neutrophils accumulation and lipid deposition. All images and statistical analysis were carried out after feeding zebrafish with red fluorescently labeled control or HCD diets for 6, 8 and 10 days, starting at 5 days post fertilization. *$p < 0.05$; **$p < 0.01$, Student's t-test. (For interpretation of the references to colour in this figure legend, the reader is referred to the Web version of this article.)

4. Discussion

Atherosclerosis is a chronic progressive vascular disease that takes decades to develop into advanced plaques in humans. The early development of atherosclerosis is believed to follow a paradigm of endothelial cell dysfunction, lipid deposition, inflammatory cell recruitment and foam cell formation [4]. However, direct imaging evidence of early development of atherosclerosis remains scarce, because it needs months to observe disease progression only with anatomy, in currently widely used mouse or rabbit models. With the zebrafish larvae model, early development of atherosclerosis can be easily studied in a few days in the optically transparent zebrafish body with a fluorescent microscope, because of the rapid development *in vitro* and the excellent characteristics as model of lipid metabolism, to study the pathological important events in early-stage atherogenesis [11]. In the present study, through chronological visualization of the sequence of these early events in live transgenic zebrafish larvae, we found that hypercholesterolemia induced endothelial inflammation (6 days post HCD feeding) preceded myeloid cells (specifically neutrophils) accumulation (8 days post HCD feeding) and lipid deposition (10 days post HCD feeding) in vascular vessels. Lipid deposition was the latest event during this process. These findings emphasized the importance of endothelial inflammation during early development of atherosclerosis.

Endothelial dysfunction caused by nitric oxide reduction, endothelial pro-inflammatory activation or hemodynamics is an important contributor to the pathobiology of atherosclerosis [37]. It is considered to be the early predictor of atherosclerosis [38]. Atherosclerosis is primarily considered a chronic inflammatory disease, as the vasculature hosts many complex chronic inflammation events among various inflammatory molecules [2] leading to endothelial dysfunction

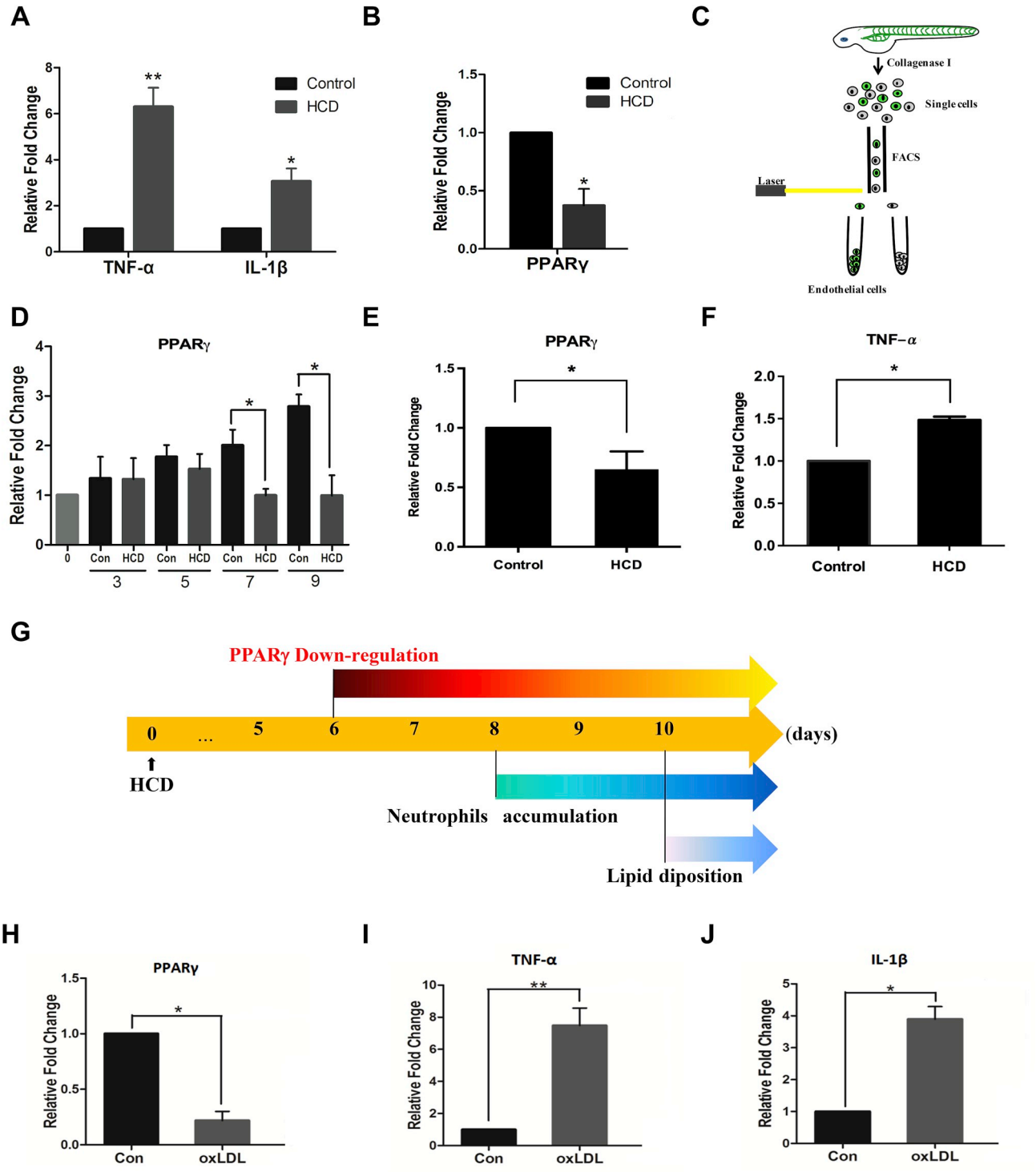

Fig. 4. *PPARγ* down-regulation in HCD-fed zebrafish larvae and endothelial cells prior to myeloid cells accumulation.
(A) Statistical analysis of pro-inflammatory genes *TNF-α*, *IL-1β* and (B) anti-inflammatory gene *PPARγ* expression in *Tg(lysc:EGFP)* larvae after feeding zebrafish with red fluorescently labeled control or HCD diets for 10 days, starting at 5 days post fertilization. (C) Schematic diagram of fluorescence-activated cell sorting (FACS) of endothelial cells in *Tg(flk1:EGFP)* larvae after feeding zebrafish with control or HCD diets. (D) Statistical analysis of *PPARγ* gene expression in sorted fluorescent endothelial cells from *Tg(flk1:EGFP)* larvae after feeding zebrafish with red fluorescently labeled control or HCD diets for 3, 5, 7 and 9 days, starting at 5 days post fertilization. (E) Statistical analysis of *PPARγ* and (F) *TNF-α* gene expression in sorted fluorescent endothelial cells from *Tg(flk1:EGFP)* larvae after feeding zebrafish with red fluorescently labeled control or HCD diets for 6 days, starting at 5 days post fertilization. (G) Schematic diagram of the chronological order of *PPARγ* gene expression change, myeloid cells accumulation and lipid deposition. (H) Statistical analysis of *PPARγ*, (I) *TNF-α* and (J) *IL-1β* gene expression in human umbilical vein endothelial cells treated with oxidized low-density lipoprotein (ox-LDL) for 24 h $*p < 0.05$; $**p < 0.01$, Student's t-test. (For interpretation of the references to colour in this figure legend, the reader is referred to the Web version of this article.)

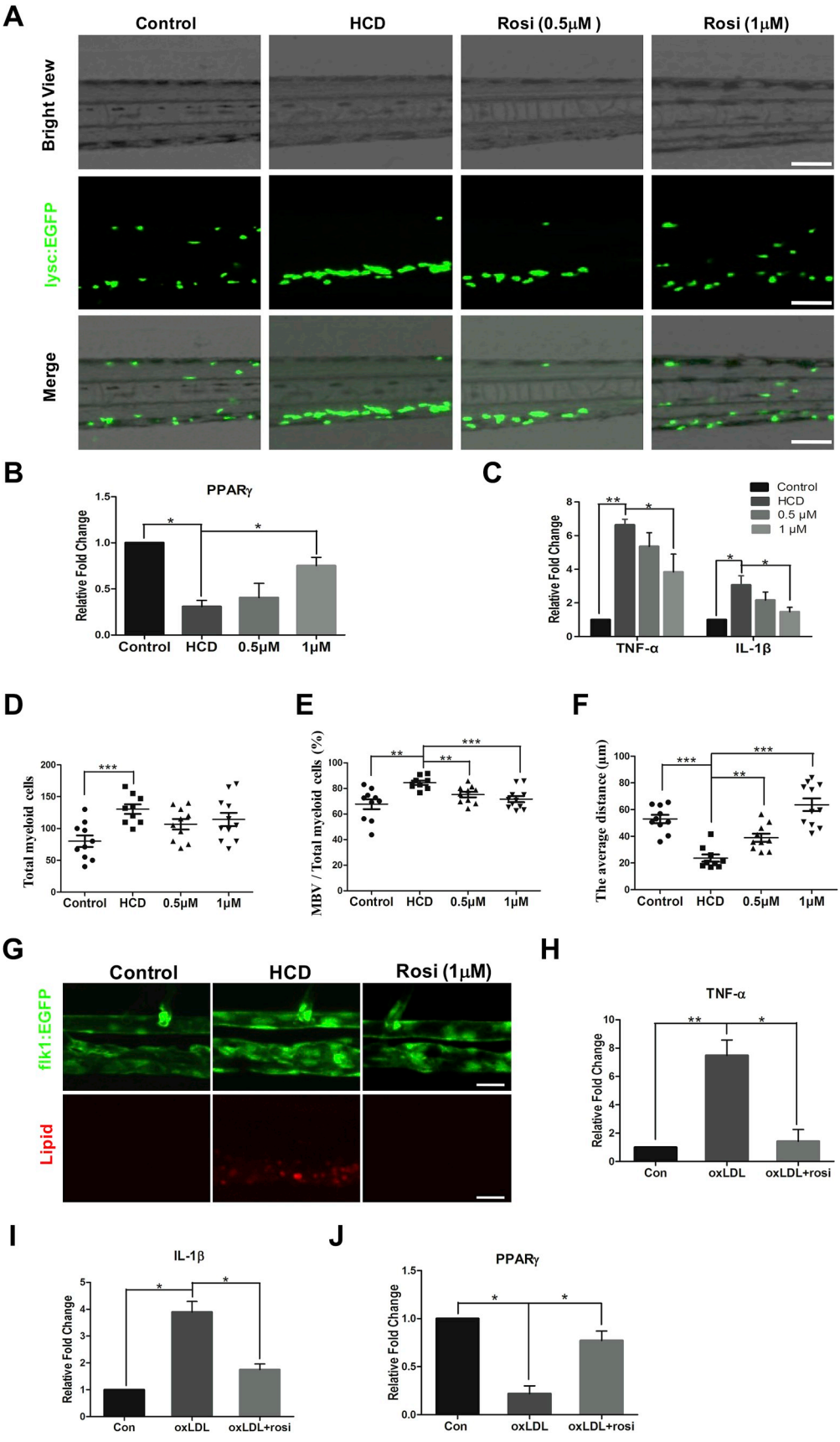

Fig. 5. *PPARγ* agonist rosiglitazone ameliorates inflammation, myeloid cells accumulation and lipid deposition in zebrafish *in vivo*.
(A) Confocal images of myeloid cells (green) accumulation between the caudal vein and dorsal aorta in *Tg(lysc:EGFP)* larvae. Scale bar, 50 μm. (B) Statistical analysis of *PPARγ*, (C) *TNF-α* and *IL-1β* gene expression. (D) Statistical analysis of total myeloid cells in the region from yolk sac to tail. (E) Percentage of myeloid cells between the caudal vein and dorsal aorta (MBV) *versus* total myeloid cells. (F) Average distance of myeloid cells to caudal vein. (G) Confocal images of lipid deposition (red) in *Tg(flk1:EGFP)* larvae vessels. All images and statistical analysis were carried out after feeding zebrafish with control or HCD diets for 10 days starting at 5 days post fertilization with or without different concentrations of *PPARγ* agonist rosiglitazone, as indicated. Scale bar, 20 μm. (H) Statistical analysis of *TNF-α*, (I) *IL-1β* and (J) *PPARγ* gene expression in human umbilical vein endothelial cells treated with oxidized low-density lipoprotein (ox-LDL) or ox-LDL and rosiglitazone (1 μM) for 24 h*$p < 0.05$; **$p < 0.01$; ***$p < 0.001$, Student's t-test. (For interpretation of the references to colour in this figure legend, the reader is referred to the Web version of this article.)

[39,40]. Accumulating evidence has demonstrated that endothelial dysfunction could be induced by interference with inflammatory molecules like *PPARγ* [41] and *TNF-α* [42,43]. In this study, we revealed that hypercholesterolemia induced endothelial dysfunction was characterized by endothelial inflammation, which was featured by the downregulated expression of *PPARγ* and upregulated expression of

TNF-α and *IL-1β*. This was confirmed by detecting their expression in FACS-sorted endothelial cells from *Tg(flk1:EGFP)* transgenic larvae fed by HCD for 6 days.

PPARγ expression in endothelial cells plays an important role in endothelial dysfunction [44,45]. *PPARγ* signal mediates activation of endothelial nitric oxide synthase (eNOS) [46], inhibits the expression of cellular adhesion molecules and reduces inflammatory cells migration and adhesion to atherosclerotic plaques [47]. Our results showed that the *PPARγ* agonist, rosiglitazone, significantly alleviated the inflammation in vasculatures and inhibited HCD-induced myeloid cells recruitment and lipid deposition. It is similar to the previous results in the rabbit model treated with rosiglitazone, while the authors thought this benefit from increased high-density lipoprotein [48]. *PPARγ* also regulates lipid and glucose utilization excepting inflammatory responses in many tissues and expresses not only in vascular endothelial cells, but also the adipose tissue [49]. However, in our study we did not regard that adipocytes participated in the early development of atherosclerosis because we did not find the accumulation of myeloid cells near adipocytes, and the mass of adipose tissue increase in HCD-fed zebrafish larvae. In addition, adipose lineage markers (*Leptin-α* and fatty acid-binding protein-11α) had no obvious alternations.

Studies have shown that cholesterol can affect *PPARγ* expression by T-box (Tbx) transcription factor [50], long noncoding RNA (lncRNA) [51] and microRNA [52]. In addition, endothelial-specific low-density lipoprotein receptor related protein 1 (LRP1) can interact with PPARγ, acting as its transcriptional co-activator in endothelial cells [53]. *Tbx20* could directly regulate *PPARγ* expression, as shown by *Tbx20* knockdown and *PPARγ* inhibition, which significantly reversed the protective effect *of Tbx20* in HUVECs [50]. Ox-LDL markedly decreased lncRNA AC096664.3 in vascular smooth muscle cells (VSMCs) and THP-1 macrophages and downregulation of lncRNA AC096664.3 reduced ABCG1 expression through inhibiting the expression of *PPARγ*, which led to an increase in total and free cholesterol in VMSCs [51]. Downregulation of miR-17–5p significantly reduced the production of inflammatory cytokines, inhibited lipid accumulation and activated *PPARγ* in macrophages of $ApoE^{-/-}$ mice fed a high cholesterol diet [52].

TNF-α and IL-1β induce the expression of neutrophil chemotactic factors in HUVEC [54] and neutrophil recruitment [55]. Combined with our evidence, we speculate that the chronological events in early atherosclerosis are endothelial inflammation, neutrophils accumulation, and lipid deposition. Then, macrophages may be recruited and infiltrate to lesions as found in human autopsy subjects and other models [27,28]. These dynamic and visual evidence *in vivo* is difficult to obtain *in vitro* or in other experimental models like mice or rabbits.

In summary, we chronologically discriminated the important events during the early development of atherosclerosis *in vivo* in transgenic zebrafish fed HCD. We revealed that endothelial inflammation occurred prior to myeloid cells (specifical neutrophils), accumulation, and myeloid cells accumulation was earlier than lipid deposition in vasculatures. We also found that downregulation of *PPARγ* expression in endothelial cells played a critical role in triggering these events. The administration of rosiglitazone (*PPARγ* agonist) significantly inhibited HCD-induced inflammation, myeloid cells accumulation and lipid deposition. Thus, we not only revealed the central role of HCD-induced endothelial cell inflammation during the initial stage of atherosclerosis, but also provided clues to enhance the therapy of atherosclerosis. Moreover, once again our study reinforces that zebrafish is an excellent *in vivo* experimental model for investigating the early events of atherosclerosis and vascular inflammation, and drug discovery targeting at atherogenesis.

Financial support

This study was supported by the National Natural Science Foundation of China (Grant IDs: 81272216 and 81171956), China.

Author contributions

Han-shuo Yang designed experiments; Hui Luo, Qi-qi Li, Ni Wu, Yu-ge Shen, Wei-ting Liao, Yun Yang, E Dong, Gui-min Zhang, Bin-rui Liu, Xiao-zhu Yue and Han-shuo Yang carried out experiments and analyzed experimental results. Hui Luo, Qi-qi Li, Ni Wu, Gui-min Zhang, Bin-rui Liu and Xiao-zhu Yue assisted to organize figures and tables. Hui Luo, Qi-qi Li, Ni Wu, Xiao-qiang Tang and Han-shuo Yang wrote the manuscript.

Declaration of competing interest

The authors declared they do not have anything to disclose regarding conflict of interest with respect to this manuscript.

Acknowledgements

We thank professor Li Li (Laboratory of Molecular Developmental Biology, School of Life Sciences, Southwest University, Chongqing, China) for kindly providing *Tg(mpx:EGFP)* and *Tg(mpeg1:EGFP)* fish.

Appendix A. Supplementary data

Supplementary data to this article can be found online at https://doi.org/10.1016/j.atherosclerosis.2019.09.017.

References

[1] P. Perel, A. Avezum, M. Huffman, et al., Reducing premature cardiovascular morbidity and mortality in people with atherosclerotic vascular disease: the world heart federation roadmap for secondary prevention of cardiovascular disease, Glob. Heart 10 (2015) 99–110, https://doi.org/10.1016/j.gheart. 2015.04.003.
[2] R. Ross, Mechanisms of disease - atherosclerosis - an inflammatory disease, N. Engl. J. Med. 340 (1999) 115–126, https://doi.org/10.1056/NEJM199901143400207.
[3] D.A. Chistiakov, A.N. Orekhov, Y.V. Bobryshev, LOX-1-Mediated effects on vascular cells in atherosclerosis, Cell. Physiol. Biochem. 38 (2016) 1851–1859, https://doi.org/10.1159/000443123.
[4] J.F. Bentzon, F. Otsuka, R. Virmani, et al., Mechanisms of plaque formation and rupture, Circ. Res. 114 (2014) 1852–1866, https://doi.org/10.1161/Circresaha.114.302721.
[5] Y. Doring, M. Drechsler, O. Soehnlein, et al., Neutrophils in atherosclerosis: from mice to man, Arterioscler. Thromb. Vasc. Biol. 35 (2015) 288–295, https://doi.org/10.1161/ATVBAHA.114.3035 64.
[6] A. Pende, N. Artom, M. Bertolotto, et al., Role of neutrophils in atherogenesis: an update, Eur. J. Clin. Investig. 46 (2016) 252–263, https://doi.org/10.1111/eci.12566.
[7] O. Soehnlein, Multiple roles for neutrophils in atherosclerosis, Circ. Res. 110 (2012) 875–888, https://doi.org/10.1161/CIRCRESAHA.111.257535.
[8] M. Drechsler, R.T. Megens, M. van Zandvoort, et al., Hyperlipidemia-triggered neutrophilia promotes early atherosclerosis, Circulation 122 (2010) 1837–1845, https://doi.org/10.1161/CIRCULATIONAHA.11 0.961714.
[9] O. Soehnlein, L. Lindbom, C. Weber, Mechanisms underlying neutrophil-mediated monocyte recruitment, Blood 114 (2009) 4613–4623, https://doi.org/10.1182/blood-2009-06-221630.
[10] I.F. Charo, R. Taub, Anti-inflammatory therapeutics for the treatment of atherosclerosis, Nat. Rev. Drug Discov. 10 (2011) 365–376, https://doi.org/10.1038/nrd3444.
[11] K. Stoletov, L.H. Fang, S.H. Choi, et al., Vascular lipid accumulation, lipoprotein oxidation, and macrophage lipid uptake in hypercholesterolemic zebrafish, Circ. Res. 104 (2009) 952–U980, https://doi.org/10.1161/Circresaha.108.189803.
[12] A. Seth, D.L. Stemple, I. Barroso, The emerging use of zebrafish to model metabolic disease, Dis. Model Mech. 6 (2013) 1080–1088, https://doi.org/10.1242/dmm.011346.
[13] C.L. Pinto, S.M. Kalasekar, C.W. McCollum, et al., Lxr regulates lipid metabolic and visual perception pathways during zebrafish development, Mol. Cell. Endocrinol. 419 (2016) 29–43, https://doi.org/10.1016/j.mce.2015.09.030.
[14] J.D. Carten, M.K. Bradford, S.A. Farber, Visualizing digestive organ morphology and function using differential fatty acid metabolism in live zebrafish, Dev. Biol. 360 (2011) 276–285, https://doi.org/10.1016/j.ydbio.2011.09.010.
[15] J.L. Anderson, J.D. Carten, S.A. Farber, Zebrafish lipid metabolism: from mediating early patterning to the metabolism of dietary fat and cholesterol, Methods Cell Biol. 101 (2011) 111–141, https://doi.org/10.1016/B978-0-12-387036-0.00005-0.
[16] L.H. Fang, R. Harkewicz, K. Hartvigsen, et al., Oxidized cholesteryl esters and phospholipids in zebrafish larvae fed a high cholesterol diet macrophage binding and activation, J. Biol. Chem. 285 (2010) 32343–32351, https://doi.org/10.1074/jbc.M110.137257.
[17] L.H. Fang, S.R. Green, J.S. Baek, et al., In vivo visualization and attenuation of

oxidized lipid accumulation in hypercholesterolemic zebrafish, J. Clin. Investig. 121 (2011) 4861–4869, https://doi.org/10.1172/JCI5 7755.
[18] C. Zhao, G.A. Gomez, Y. Zhao, et al., ETV2 mediates endothelial transdifferentiation of glioblastoma, Signal Transduct. Target. Ther. 3 (2018) 4, https://doi.org/10.1038/s41392-018-0007-8.
[19] C. Zhao, W. Zhang, Y. Zhao, et al., Endothelial cords promote tumor initial growth prior to vascular function through a paracrine mechanism, Sci. Rep. 6 (2016), https://doi.org/10.1038/srep 19404 19404.
[20] B. Baudin, A. Bruneel, N. Bosselut, et al., A protocol for isolation and culture of human umbilical vein endothelial cells, Nat. Protoc. 2 (2007) 481–485, https://doi.org/10.1038/nprot.2007.54.
[21] D.J. Sanchez, D.J. Steger, N. Skuli, et al., PPARgamma is dispensable for clear cell renal cell carcinoma progression, Mol. Metab. 14 (2018) 139–149, https://doi.org/10.1016/j.molmet.2018.05.013.
[22] M. Nasri, A. Karimi, M. Allahbakhshian Farsani, Production, purification and titration of a lentivirus-based vector for gene delivery purposes, Cytotechnology 66 (2014) 1031–1038, https://doi.org/10.1007/s 10616-013-9652-5.
[23] E.M. Dunn, E.J. Billquist, A.L. VanderStoep, et al., Dual roles of fer kinase are required for proper hematopoiesis and vascular endothelium organization during zebrafish development, Biology 6 (2017), https://doi.org/10.3390/biology6040040.
[24] A.E. Mullick, K. Soldau, W.B. Kiosses, et al., Increased endothelial expression of Toll-like receptor 2 at sites of disturbed blood flow exacerbates early atherogenic events, J. Exp. Med. 205 (2008) 373–383, https://doi.org/10.1084/jem.20071096.
[25] L. Liberale, F. Dallegri, F. Montecucco, et al., Pathophysiological relevance of macrophage subsets in atherogenesis, Thromb. Haemost. 117 (2017) 7–18, https://doi.org/10.1160/Th16-08-0593.
[26] C. Hall, M.V. Flores, T. Storm, et al., The zebrafish lysozyme C promoter drives myeloid-specific expression in transgenic fish, BMC Dev. Biol. 7 (2007) 42, https://doi.org/10.1186/1471-213X-7-42.
[27] Y. Nakashima, H. Fujii, S. Sumiyoshi, et al., Early human atherosclerosis - accumulation of lipid and proteoglycans in intimal thickenings followed by macrophage infiltration, Arterioscler. Thromb. Vasc. 27 (2007) 1159–1165, https://doi.org/10.1161/Atvbaha.106.134080.
[28] Y. Nakashima, T.N. Wight, K. Sueishi, Early atherosclerosis in humans: role of diffuse intimal thickening and extracellular matrix proteoglycans, Cardiovasc. Res. 79 (2008) 14–23, https://doi.org/10.1093/cvr/cv n099.
[29] J.R. Mathias, B.J. Perrin, T.X. Liu, et al., Resolution of inflammation by retrograde chemotaxis of neutrophils in transgenic zebrafish, J. Leukoc. Biol. 80 (2006) 1281–1288, https://doi.org/10.1189/jlb.0506346.
[30] F. Ellett, L. Pase, J.W. Hayman, et al., mpeg1 promoter transgenes direct macrophage-lineage expression in zebrafish, Blood 117 (2011) e49–56, https://doi.org/10.1182/blood-2010-10-314120.
[31] A. Zakrzewska, C. Cui, O.W. Stockhammer, et al., Macrophage-specific gene functions in Spi1-directed innate immunity, Blood 116 (2010) e1–11, https://doi.org/10.1182/blood-2010-01-262873.
[32] X. Jing, S.S. Chen, W. Jing, et al., Diagnostic potential of differentially expressed Homer1, IL-1beta, and TNF-alpha in coronary artery disease, Int. J. Mol. Sci. 16 (2014) 535–554, https://doi.org/10.3390/ijms16010535 6.
[33] J. Kotlinowski, A. Jozkowicz, PPAR gamma and angiogenesis: endothelial cells perspective, J. Diabetes Res. 2016 (2016), https://doi.org/10.1155/2016/8492353 8492353.
[34] M.A. Bouhlel, B. Derudas, E. Rigamonti, et al., PPARgamma activation primes human monocytes into alternative M2 macrophages with anti-inflammatory properties, Cell Metabol. 6 (2007) 137–143, https://doi.org/10.1016/j.cmet.2007.06.010.
[35] M. Lehrke, M.A. Lazar, The many faces of PPARgamma, Cell 123 (2005) 993–999, https://doi.org/10.1016/j.cell.2005.11.026.
[36] S.W. Coppack, Pro-inflammatory cytokines and adipose tissue, Proc. Nutr. Soc. 60 (2001) 349–356.
[37] M.A. Gimbrone Jr., G. Garcia-Cardena, Endothelial cell dysfunction and the pathobiology of atherosclerosis, Circ. Res. 118 (2016) 620–636, https://doi.org/10.1161/CIRCRESAHA.115.306301.
[38] M. Mudau, A. Genis, A. Lochner, et al., Endothelial dysfunction: the early predictor of atherosclerosis, Cardiovasc. J. Afr. 23 (2012) 222–231, https://doi.org/10.5830/CVJA-2011-068.
[39] C.M. Steyers 3rd, F.J. Miller Jr., Endothelial dysfunction in chronic inflammatory diseases, Int. J. Mol. Sci. 15 (2014) 11324–11349, https://doi.org/10.3390/ijms150711324.
[40] E. Horio, T. Kadomatsu, K. Miyata, et al., Role of endothelial cell-derived angptl2 in vascular inflammation leading to endothelial dysfunction and atherosclerosis progression, Arterioscler. Thromb. Vasc. Biol. 34 (2014) 790–800, https://doi.org/10.1161/ATVBAHA.113.303116.
[41] C. Hu, K.T. Lu, M. Mukohda, et al., Interference with PPARgamma in endothelium accelerates angiotensin II-induced endothelial dysfunction, Physiol. Genom. 48 (2016) 124–134, https://doi.org/10.1152/physiolgenomics.00087.2015.
[42] S. Chia, M. Qadan, R. Newton, et al., Intra-arterial tumor necrosis factor-alpha impairs endothelium-dependent vasodilatation and stimulates local tissue plasminogen activator release in humans, Arterioscler. Thromb. Vasc. Biol. 23 (2003) 695–701, https://doi.org/10.1161/01.ATV.000 0065195.22904 FA.
[43] P. Wang, Z.F. Ba, I.H. Chaudry, Administration of tumor necrosis factor-alpha in vivo depresses endothelium-dependent relaxation, Am. J. Physiol. 266 (1994) H2535–H2541, https://doi.org/10.1152/ajpheart.1994.266.6.H2535.
[44] S.Z. Duan, M.G. Usher, R.M. Mortensen, Peroxisome proliferator-activated receptor-gamma-mediated effects in the vasculature, Circ. Res. 102 (2008) 283–294, https://doi.org/10.1161/Circres aha.107.164384.
[45] C.K. Glass, S. Ogawa, Combinatorial roles of nuclear receptors in inflammation and immunity, Nat. Rev. Immunol. 6 (2006) 44–55, https://doi.org/10.1038/nri1748.
[46] C. Maccallini, A. Mollica, R. Amoroso, The positive regulation of eNOS signaling by PPAR agonists in cardiovascular diseases, Am. J. Cardiovasc. Drugs 17 (2017) 273–281, https://doi.org/10.1007/s40256-0 17-0220-9.
[47] V. Pasceri, H.D. Wu, J.T. Willerson, et al., Modulation of vascular inflammation in vitro and in vivo by peroxisome proliferator-activated receptor-gamma activators, Circulation 101 (2000) 235–238, https://doi.org/10.1161/01.Cir.101.3.235.
[48] C. Lii, Y. Tu, T.R. Liu, et al., Rosiglitazone attenuates atherosclerosis and increases high-density lipoprotein function in atherosclerotic rabbits, Int. J. Mol. Med. 35 (2015) 715–723, https://doi.org/10.3892/ijmm.2015. 2072.
[49] C. Janani, B.D. Ranjitha Kumari, PPAR gamma gene–a review, Diabetes, Metab. Syndrome 9 (2015) 46–50, https://doi.org/10.1016/j.dsx.2014.09.015.
[50] T. Shen, Y. Zhu, J. Patel, et al., T-box20 suppresses oxidized low-density lipoprotein-induced human vascular endothelial cell injury by upregulation of PPAR-gamma, Cell. Physiol. Biochem. 32 (2013) 1137–1150, https://doi.org/10.1159/000354514.
[51] B.M. Xu, L. Xiao, C.M. Kang, et al., LncRNA AC096664.3/PPAR-gamma/ABCG1-dependent signal transduction pathway contributes to the regulation of cholesterol homeostasis, J. Cell. Biochem. 120 (2019) 13775–13782, https://doi.org/10.1002/jcb.28650.
[52] L. Tan, L. Liu, Z. Jiang, et al., Inhibition of microRNA-17-5p reduces the inflammation and lipid accumulation, and up-regulates ATP-binding cassette transporterA1 in atherosclerosis, J. Pharmacol. Sci. 139 (2019) 280–288, https://doi.org/10.1016/j.jphs.2018.11.012.
[53] H. Mao, P. Lockyer, L. Li, et al., Endothelial LRP1 regulates metabolic responses by acting as a co-activator of PPARgamma, Nat. Commun. 8 (2017), https://doi.org/10.1038/ncomms14960 14960.
[54] R.M. Strieter, S.L. Kunkel, H.J. Showell, et al., Endothelial cell gene expression of a neutrophil chemotactic factor by TNF-alpha, LPS, and IL-1 beta, Science (New York, N.Y.) 243 (1989) 1467–1469.
[55] S. Sheikh, M. Rahman, Z. Gale, et al., Differing mechanisms of leukocyte recruitment and sensitivity to conditioning by shear stress for endothelial cells treated with tumour necrosis factor-alpha or interleukin-1beta, Br. J. Pharmacol. 145 (2005) 1052–1061, https://doi.org/10.1038/sj.bjp.0706281.